Nanosilicon-Coated Graphene Granules as Anodes for Li-Ion Batteries

*Kara Evanoff, Alexandre Magasinski, Junbing Yang, and Gleb Yushin**

Increased concern regarding environmental pollution from combustion power sources combined with the shortage of oil reserves and the growing demand for portable electronics and powered devices has generated considerable research activity to develop Li-ion batteries with greatly enhanced energy density.[1] Historically, the Li-ion anode has been composed of graphitic carbon. At full lithiation, graphite can intercalate one Li atom per six carbon atoms (LiC_6) for a theoretical capacity of 372 $mAh \cdot g^{-1}$.[2]

Substituting graphene for graphite to increase the number of lithiation sites and gain higher capacity has been explored.[3] The common shortcomings of graphene-based anodes include very high irreversible capacity losses at the first cycle, low Coulombic efficiency (CE) in subsequent cycles and limited overall stability caused by the separation of graphene layers, which make graphene unsuitable as a replacement to the current graphite anode technology. Composite electrodes consisting of graphene nanosheets and carbon nanotubes and/or fullerenes have shown to increase discharge capacity but failed to improve its stability to industrially useful levels.[3c]

The application of elements that electrochemically alloy with Li at room temperature offers an alternative solution to the high capacity anode demand.[4] Si has received particular attention due to its highest gravimetric capacity for Li.[5] The challenge to achieve a stable performance of the Li alloying elements originates from the large volume changes occurring during the Li insertion/extraction processes[5g,5i,6] The Li-Si system can expand/contract during alloying/dealloying by as much as 300% by volume[7] after forming $Li_{15}Si_4$ with a theoretical capacity of 3579 $mAh \cdot g^{-1}$.[6] These cyclical volume changes can generate stresses in the electrode material, forming cracks and breaks in electrical conductivity.[8] In addition, conventional battery construction cannot accommodate electrode volume changes in excess of 6–8%. The use of Si nanoparticles, often combined with a high binder and C additive content,[5c,5h] may overcome some of these limitations at the expense of lowering the volumetric capacity.

To mitigate the detrimental effects of volume changes in Si, much effort has been undertaken to produce composite electrodes consisting of a high capacity material and various carbons at the nanoscale.[4b,5g,5i,9] Early Si-C composite electrodes were mostly fabricated by the decomposition of C- and Si- containing precursors or through mechanical mixing and have not exhibited acceptable performance[9b,10] due to limited porosity available for Si volume changes and non-uniform material properties at the nanoscale. Recent work has demonstrated that significantly better performance could be achieved if the composite materials contain uniformly distributed Si, C, and interconnected pores.[5a,5e,5g,5i,9f,9g]

Several studies analyzed the performance of graphene mixed with high capacity nanoparticles of Sn[9c] or Si[11] using physical mixing or solution-based methods. In spite of the noticeable improvements over the pure graphene performance, these studies demonstrated several shortcomings. The high surface area led to very large irreversible capacity losses and low CE at the first (<73%) and the subsequent 30 cycles (80–94%). The anode stability was moderate with ~30% losses during the first 30–100 cycles. In the case of Sn, the capacity improvements were also moderate, ~500 $mAh \cdot g^{-1}$ after 100 cycles[9c], only a slight increase beyond theoretical capacity for graphite and less than the proposed theoretical capacity of graphene (744 $mAh \cdot g^{-1}$).

Here, we present an alternative method to synthesize porous nanosilicon- and graphene-containing nanocomposites with the specific Li extraction capacity in excess of 2000 $mAh \cdot g^{-1}$ and stable performance for over 150 cycles. In contrast to prior work on graphene mixed with Si[11], we employ vapor deposition methods in our synthesis, which allowed us to reduce the graphene surface area by over 100 times and achieve an average CE in excess of 99%. In contrast to prior work on Si nanoparticles deposited on carbon black[5i] or graphite[9a,9d,9e], we study continuous Si films conformally deposited on the graphene sheets, a feature not previously found in the literature. The proposed synthesis route and the developed architecture of three-dimensional (3D) porous particles composed of curved two-dimensional (2D) nano-sized layers may provide unique benefits. The prior work on thin film batteries[12] showed that during Li insertion large area Si films mostly accommodate the volume changes via variation in thickness. Therefore, the changes in the external surface area during cycling can be minimized and, thus, formation of a stable solid electrolyte interphase (SEI) should be easier to achieve than in Si nanoparticles or nanowires, which experience very large external surface area changes during insertion/extraction of Li. Additionally, the high specific surface area of graphene allows rapid Si deposition, which is important for practical applications. Finally, the tunable spacing between individual graphene layers permits for Si film depositions of various thicknesses and thus optimization of the composite for either high energy or high power

K. Evanoff, Dr. A. Magasinski, Prof. G. Yushin
School of Materials Science and Engineering
Georgia Institute of Technology
771 Ferst Drive, Atlanta, GA 30332–0245, USA
E-mail: yushin@gatech.edu
Dr. J. Yang
Chemical Sciences & Engineering Division
Argonne National Laboratory
9700 S. Cass Avenue, Argonne, IL 60439, USA

DOI: 10.1002/aenm.201100071

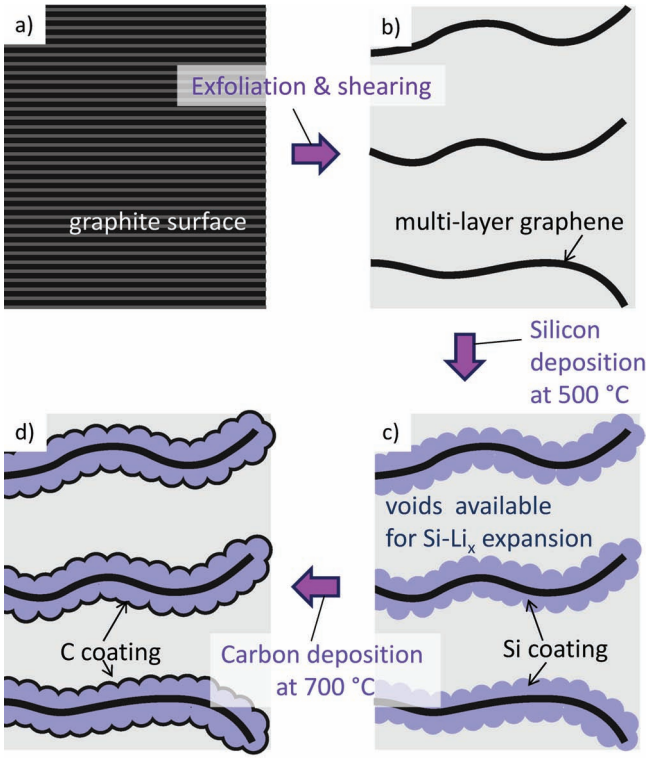

Figure 1. Schematic of C-Si-graphene composite formation: a) natural graphite is transformed to b) graphene and then c) coated by Si nanoparticles and d) a thin C layer.

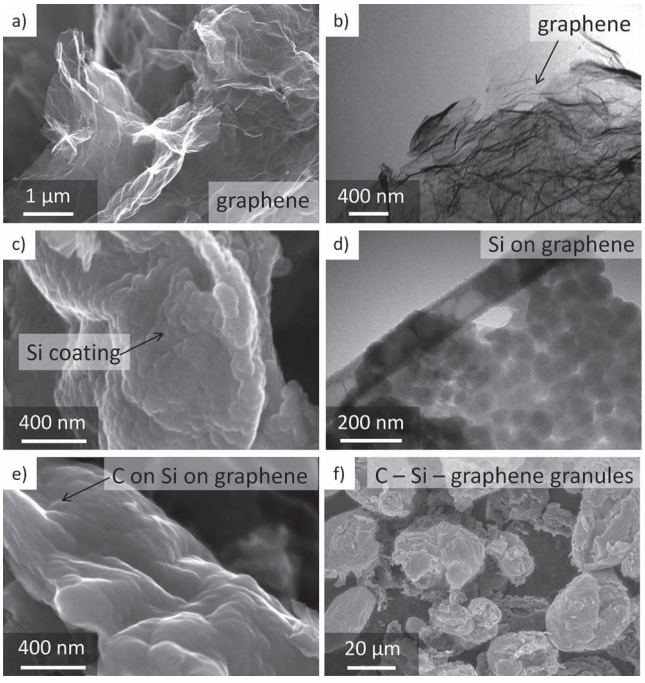

Figure 2. Structure of the Si-graphene materials. a, c, e, f) SEM and b, d) TEM micrographs of a, b) graphene, c, d) Si-coated graphene, and e, f) C-Si-graphene granules.

applications. While only a Si-containing composite is demonstrated, the synthesis techniques are applicable for other high capacity materials that can be conformally coated on graphene.

Figure 1 shows the process flow for the reported formation of the nanocomposite powder. First, graphene is produced via exfoliation of a natural graphite followed by ultrasonic shearing. While mechanical shearing produces graphene of very high quality, the process is not very scalable. Ultrasonic treatment allows scalable graphene production with significantly higher yield. Second, the produced graphene was uniformly coated with Si via SiH_4 decomposition at 500 °C and finally with C via decomposition of C_3H_6 at 700 °C. Carbon coating was deposited to reduce Si oxidation and improve anode stability.[5g–i]

Scanning electron microscopy (SEM) and transmission electron microscopy (TEM) images show the evolution of the composite material morphology (**Figure 2**). The deposited Si nanoparticles uniformly coat the smooth graphene sheets (Figure 2a, b) forming a rough continuous surface (Figure 2c,d). No crystallites were observed in the TEM images, indicating amorphous structure of Si. The carbon layer uniformly coats the Si surface reducing the surface roughness (Figure 2e). The produced composite particles (Figure 2f) retain the original 10–30 µm size of the graphene agglomerates.

Raman spectroscopy (**Figure 3**a) revealed the synthesized graphene to show nearly the same spectra as commercially available purified exfoliated graphite (PEG), suggesting that a large portion of the produced graphene has more than 5 layers.[13] Characteristic Raman peaks for carbon materials are the disorder-induced D band at ~1350 cm^{-1}, the graphitic G band at ~1580 cm^{-1}, the second order G' band (also known as the 2D band) at ~2700 cm^{-1} and D" (also known as the D+G band) at ~2900 cm^{-1}.[13,14] The large D peak and the small relative intensity of the 2D peak indicate a high concentration of defects, dangling bonds, and structural disorder present.[13,15] These defects likely served as nucleation sites for Si nanoparticle deposition and allowed uniform coating formation (Figure 2). Raman spectroscopy verified the deposition of Si (~520 cm^{-1}). The lack of carbon peaks in the Si-coated sample (Figure 3a) indicates conformal Si deposition, supporting SEM and TEM measurements (Figure 2). The C deposition was confirmed by the reappearance of D and G peaks (Figure 3a). The small shift in the Si band suggests stresses caused by the difference in the thermal expansion of Si and C.

X-ray diffraction (XRD) studies (Figure 3b) provided additional information about the structural changes accompanying the synthesis steps. The XRD pattern of graphene showed weak graphite peaks ~26° and ~43°. Those peaks were suppressed after Si coating. The very broad Si peaks indicate amorphous structure of Si on the graphene surface. Carbon deposition at a higher temperature caused crystallization of Si, as evidenced by the formation of diffraction peaks (Figure 3b).

Analysis of the N_2 sorption isotherm of the produced graphene (Figure 3c) indicated its very high specific surface area (940 $m^2 \cdot g^{-1}$) and the presence of micropores. The Si and C deposition eliminated the smallest pores and reduced the surface area of the produced composite to ~ 5 $m^2 \cdot g^{-1}$.

Electrochemical performance evaluation of the produced composite was performed in the potential range from 10 mV to 1 V in 2016-type coin cells with a metallic Li foil counter electrode. The first cycle recorded at the low current density of

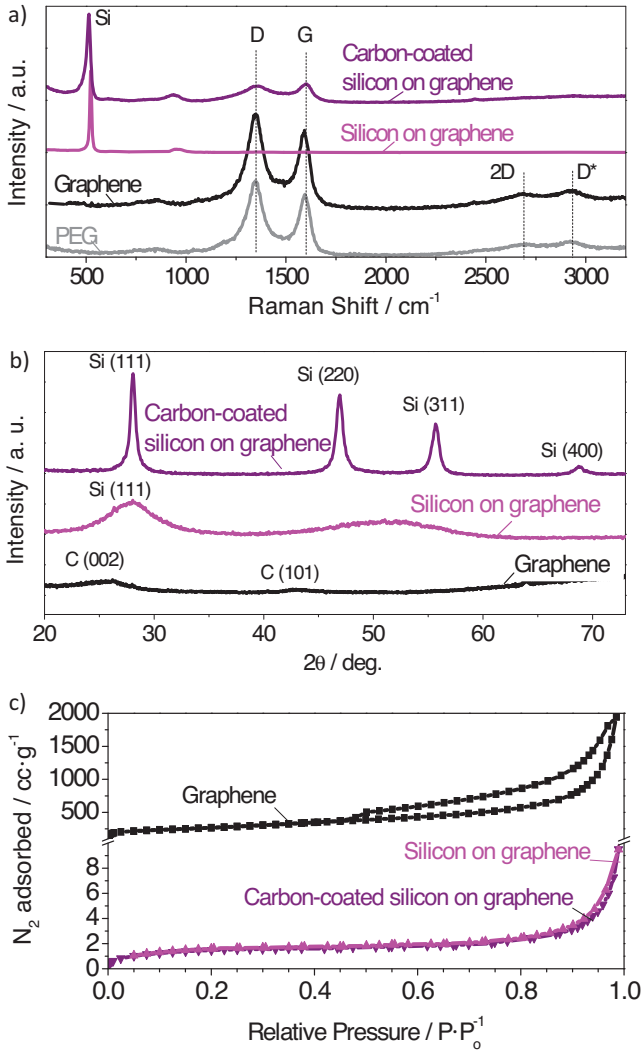

Figure 3. Characterization of the graphene and graphene-based materials by a) Raman spectroscopy, b) X-ray diffraction and c) N_2 physisorption.

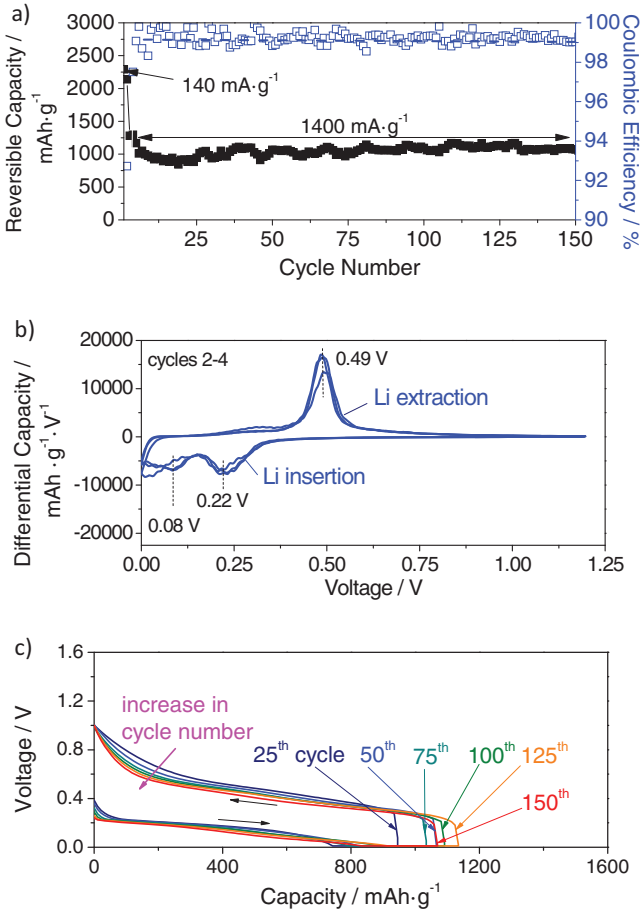

Figure 4. Electrochemical performance of the C-Si-graphene electrode: a) capacity (per mass of the composite) and Coulombic efficiency as a function of cycle number, b) a differential capacity plot and c) charge-discharge profiles for selected cycles.

140 mA·g^{-1} showed a high reversible discharge capacity of ~2300 mAh·g^{-1} (1080 mAh·cc^{-1}) (**Figure 4**a). This reversible capacity is over six times greater than the theoretical capacity of graphite, indicating a high degree of Li alloying with Si. Increasing the current density to 1400 mA·g^{-1} resulted in the reduction of the average specific reversible capacity to ~1060 mAh·g^{-1}. Stability of the produced electrodes for 150 cycles (Figure 4a) is quite remarkable considering that the Li insertion capacity and the resulting Si expansion were not limited. Another positive attribute of the produced composite is high CE (99%, on average), which is likely due to the low composite surface area (Figure 3c), planar Si geometry and its good cycle stability.

The potentials at which Li (de-)alloying occurs were examined by cyclic voltammetry (Figure 4b). Broad lithiation peaks were observed at 0.08 and 0.22 V vs. Li/Li$^+$, consistent with our earlier studies on C-coated Si.[5i] The Li was extracted from Si at 0.49 V. The peak height slightly increased after the second cycle, indicating improved cycling kinetics. Carbon delithiation occurs at potentials lower than Si and corresponding peaks are not evident in the differential capacity curves due to the significantly larger Li capacity of Si. Charge/discharge voltage profiles (Figure 4c) show transformations in the electrode during cycling. The shapes of the profiles are similar to the profiles previously reported in literature for other Si electrodes.[5i] With increasing cycling number the Li extraction profiles become more horizontal and exhibit slightly smaller overpotential, suggesting a gradual improvement in the discharge kinetics.[5f]

In summary, we have demonstrated that uniform Si and C coatings can be deposited on high surface area graphene via vapor decomposition routes. The produced Si and C-coated graphene granules exhibit specific surface area of ~5 m^2·g^{-1} and an average size of ~25 μm. The anode composed of the nanocomposite particles exhibited specific capacity in excess of 2000 mAh·g^{-1} at the current density of 140 mA·g^{-1} and excellent stability for 150 cycles, significantly exceeding the theoretical capacity of graphite and graphene. The low surface area of the composite resulted in an average Coulombic efficiency in excess of 99%. The proposed architecture of 3D porous particles composed of curved 2D layers may provide unique benefits for a number of Li alloying materials. The developed fabrication route is suitable to generate other high capacity composite electrodes.

Experimental Section

Graphene was produced from natural graphite via a multi-step process. First, a natural graphite powder (Sigma Aldrich, USA) was immersed in concentrated sulfuric acid (Sigma Aldrich, USA) for two h. The product was dried and then subjected to thermal shock treatment at 1000 °C for 30 s to obtain exfoliated graphite worms. The exfoliated graphite worms were then dispersed in deionized water and subjected to extensive ultrasonication to break down the graphite flakes and separate the graphene sheets. The dried product, graphene oxide, was reduced at 800 °C in a H_2 stream for one h to obtain the graphene powder.

Low-pressure decomposition of a high purity SiH_4 (5 wt.% in He balance; Airgas, USA) at 500 °C was utilized to deposit Si onto graphene. A thin layer of amorphous carbon was then deposited on the Si coated graphene via atmospheric pressure decomposition of high purity C_3H_6 (Airgas, USA) at 700 °C for 45 min. A mineral oil bubbler was placed in line with the gas exhaust. The produced composite contained ~60 wt.% Si. The Si and C contents were calculated via mass change measurements after the corresponding depositions and verified using thermogravimetric analysis.

The material morphology was examined by SEM (Hitachi 4700, Japan) and TEM (JEOL 100 CX, Japan). SEM images were taken using a 10 kV accerlating voltage and a 5–7 mm working distance. TEM studies were performed at an accelerating voltage of 100 kV. XRD (PANalytical X'Pert PRO Alpha-1, USA, Cu Kα source) and Raman spectroscopy (Horiba Jvon spectrometer, USA, 532 nm laser) were utilized for elemental and structural analysis. The XRD parameters were as follows: 45 kV accelerating voltage, 40 mA current, 0.033° 2θ-step size, and 120 s record time. Materials Data, Inc. Jade version 8 with ICDD PDF-4 database was utilized for analysis. For Raman spectroscopy, an exposure time of five seconds with a 0.6 filter, 400 μm hole, 100 μm slit and 600 grating was used. N_2 physisorption (Micromeritics TriStar II 3020, USA) at –196 °C allowed for the determination of the specific surface area of the initial and coated materials. Each sample was degassed in N_2 gas at 100 °C and 300 °C for at least 30 min and 8 h, respectively, prior to the measurements. The Brunauer-Emmett-Teller method was used to calculate the surface area.

The carbon and silicon coated graphene electrodes were prepared from a water-based slurry containing poly(acrylic) acid (15 wt.%) binder. After casting, the electrode was dried in a conventional oven at 70 °C for two h and in a vacuum oven at 70 °C for 8 h. Electrodes were spot-welded to the 2016-type coin cell and then assembled into half cells with a Li foil counter electrode (battery grade; Alfa Aesar, USA) in an Ar filled glovebox (<1 ppm H_2O, O_2). An electrolyte solution consisting of 1.0 M $LiPF_6$ in carbonates (Novolyte Technologies, USA) was used. Galvanostatic charge-discharge cycling was performed on an Arbin SB2000 (Arbin Instruments, USA) between 10 mV and 1V. The Coulombic efficiency was calculated by taking a ratio of the capacity after Li dealloying to the capacity after Li alloying. Cyclic voltammetry in the potential window of 0 to 1.2 V at a rate of 0.014 $mV \cdot s^{-1}$ was performed on a Solartron 1480 (Solartron Analytical, USA) multichannel potentiostat.

Acknowledgements

This work was partially supported by NASA via Contract No.NNC08CB01C. We thank B. Hertzberg, I. Kovalenko, B. Zhdyrko, I. Luzinov, and T. Fuller for helpful discussions.

Received: February 17, 2011
Published online: April 21, 2011

[1] M. Armand, J.-M. Tarascon, *Nature* **2008**, *451*, 652–657.
[2] J. R. Dahn, T. Zheng, Y. Liu, J. S. Xue, *Science* **1995**, *270*, 590–593.
[3] a) M. Liang, L. Zhi, *J. Mater. Chem.* **2009**, *19*, 5871–5878; b) E. Pollak, B. Geng, K.-J. Jeon, I. T. Lucas, T. J. Richardson, F. Wang, R. Kostecki, *Nano Lett.* **2010**, *10*, 3386–3388; c) E. Yoo, J. Kim, E. Hosono, H. Zhou, T. Kudo, I. Honma, *Nano Lett.* **2008**, *8*, 2277–2282; d) D. Pan, S. Wang, B. Zhao, M. Wu, H. Zhang, Y. Wang, Z. Jiao, *Chem. Mater.* **2009**, *21*, 3136–3142.
[4] a) M. N. Obrovac, L. Christensen, D. Ba Le, J. R. Dahn, *J. Electrochem. Soc.* **2007**, *154*, A849-A855-; b) R. A. Huggins, *J. Power Sources* **1999**, *81–82*, 13–19.
[5] a) H. Kim, J. Cho, *Nano Lett.* **2008**, *8*, 3688–3691; b) C. K. Chan, H. L. Peng, G. Liu, K. McIlwrath, X. F. Zhang, R. A. Huggins, Y. Cui, *Nat. Nanotechnol.* **2008**, *3*, 31–35; c) S. D. Beattie, D. Larcher, M. Morcrette, B. Simon, J. M. Tarascon, *J. Electrochem. Soc.* **2008**, *155*, A158–A163; d) M. N. Obrovac, L. J. Krause, *J. Electrochem. Soc.* **2007**, *154*, A103-A108; e) H. Kim, B. Han, J. Choo, J. Cho, *Angew. Chem. Int. Ed.* **2008**, *47*, 10151–10154; f) R. Chandrasekaran, A. Magasinski, G. Yushin, T. F. Fuller, *J. Electrochem. Soc.* **2010**, *157*, A1139-A1151; g) B. Hertzberg, A. Alexeev, G. Yushin, *J. Am. Chem. Soc.* **2010**, *132*, 8548–8549; h) A. Magasinki, B. Zdyrko, I. Kovalenko, B. Hertzberg, I. Burtovyy, T. Fuller, I. Luzinov, G. Yushin, *ACS Appl. Mater. Interfaces* **2010**, *2*, 3004–3010; i) A. Magasinski, P. Dixon, B. Hertzberg, A. Kvit, J. Ayala, G. Yushin, *Nat. Mater.* **2010**, *9*, 353–358; j) N. Balke, S. Jesse, Y. Kim, L. Adamczyk, A. Tselev, I. N. Ivanov, N. J. Dudney, S. V. Kalinin, *Nano Lett.* **2010**, *10*, 3420–3425.
[6] M. N. Obrovac, L. Christensen, *Electrochem. Solid-State Lett.* **2004**, *7*, A93–A93.
[7] B. A. Boukamp, G. C. Lesh, R. A. Huggins, *J. Electrochem. Soc.* **1981**, *128*, 725–729.
[8] a) R. A. Huggins, W. D. Nix, *Ionics* **2000**, *6*, 57–63; b) U. Kasavajjula, C. S. Wang, A. J. Appleby, *J. Power Sources* **2007**, *163*, 1003–1039.
[9] a) V. G. Khomenko, V. Z. Barsukov, J. E. Doninger, I. V. Barsukov, *J. Power Sources* **2007**, *165*, 598–608; b) A. M. Wilson, J. R. Dahn, *J. Electrochem. Soc.* **1995**, *142*, 326–332; c) G. X. Wang, B. Wang, X. L. Wang, J. Park, S. X. Dou, H. Ahn, K. Kim, *Journal of Materials Chemistry* **2009**, *19*, 8378–8384; d) M. Holzapfel, H. Buqa, W. Scheifele, P. Novak, F. M. Petrat, *Chemical Commun.* **2005**, 1566–1568; e) M. Holzapfel, H. Buqa, F. Krumeich, P. Novak, F. M. Petrat, C. Veit, *Electrochem. Solid State Lett.* **2005**, *8*, A516-A520; f) G. X. Wang, J. H. Ahn, J. Yao, S. Bewlay, H. K. Liu, *Electrochem. Commun.* **2004**, *6*, 689–692; g) Y. S. Hu, R. Demir-Cakan, M. M. Titirici, J. O. Muller, R. Schlogl, M. Antonietti, J. Maier, *Angew. Chem. Int. Ed.* **2008**, *47*, 1645–1649.
[10] a) Y. Zhang, X. G. Zhang, H. L. Zhang, Z. G. Zhao, F. Li, C. Liu, H. M. Cheng, *Electrochim. Acta* **2006**, *51*, 4994–5000; b) X. W. Zhang, P. K. Patil, C. Wang, A. J. Appleby, F. E. Little, D. L. Cocke, *J. Power Sources* **2004**, *125*, 206–213; c) J. Xie, G. S. Cao, X. B. Zhao, *Mater. Chem. Physics* **2004**, *88*, 295–299; d) N. Dimov, S. Kugino, A. Yoshio, *J. Power Sources* **2004**, *136*, 108–114; e) Y. Zhang, Z. G. Zhao, X. G. Zhang, H. L. Zhang, F. Li, C. Liu, H. M. Cheng, *Int. J. Nanomanufacturing* **2008**, *2*, 4–15.
[11] a) S.-L. Chou, J.-Z. Wang, M. Choucair, H.-K. Liu, J. A. Stride, S.-X. Dou, *Electrochem. Commun.* **2010**, *12*, 303–306; b) J. K. Lee, K. B. Smith, C. M. Hayner, H. H. Kung, *Chem. Commun.* **2010**, *46*, 2025–2025.
[12] a) S. Ohara, J. Suzuki, K. Sekine, T. Takamura, *J. Power Sources* **2004**, *136*, 303–306; b) K. Yoshimura, J. Suzuki, K. Sekine, T. Takamura, *J. Power Sources* **2005**, *146*, 445–447; c) J. Graetz, C. C. Ahn, R. Yazami, B. Fultz, *Electrochem. Solid State Lett.* **2003**, *6*, A194–A197.
[13] A. C. Ferrari, J. C. Meyer, V. Scardaci, C. Casiraghi, M. Lazzeri, F. Mauri, S. Piscanec, D. Jiang, K. S. Novoselov, S. Roth, A. K. Geim, *Phys. Rev. Lett.* **2006**, *97*, 187401–187401.
[14] A. Ferrari, *Solid State Commun.* **2007**, *143*, 47–57.
[15] a) A. C. Ferrari, J. Robertson, *Phys. Rev. B* **2000**, *61*, 14095–14107; b) O. Beyssac, B. Goffé, J.-P. Petitet, E. Froigneux, M. Moreau, J.-N. Rouzaud, *Spectrochim. Acta Part A* **2003**, *59*, 2267–2276.